Magnons and magnetodielectric effects in $CoCr_2O_4$: Raman scattering studies

A. Sethi,[1,*] T. Byrum,[1] R. D. McAuliffe,[2] S. L. Gleason,[1] J. E. Slimak,[1] D. P. Shoemaker,[2] and S. L. Cooper[1,†]

[1]*Department of Physics and Frederick Seitz Materials Research Laboratory, University of Illinois, Urbana, Illinois 61801, USA*

[2]*Department of Materials Science and Engineering and Frederick Seitz Materials Research Laboratory, University of Illinois, Urbana, Illinois 61801, USA*

(Received 21 November 2016; revised manuscript received 11 March 2017; published 9 May 2017)

Magnetoelectric materials have generated wide technological and scientific interest because of the rich phenomena these materials exhibit, including the coexistence of magnetic and ferroelectric orders, magnetodielectric behavior, and exotic hybrid excitations such as electromagnons. The multiferroic spinel material $CoCr_2O_4$ is a particularly interesting example of a multiferroic material, because evidence for magnetoelectric behavior in the ferrimagnetic phase seems to conflict with traditional noncollinear-spin-driven mechanisms for inducing a macroscopic polarization. With the overall goal of clarifying the magnetodielectric behavior previously reported below T_C in $CoCr_2O_4$, in this paper we report an inelastic light scattering study of the magnon and phonon spectrum of $CoCr_2O_4$ as simultaneous functions of temperature, pressure, and magnetic field. Below the Curie temperature ($T_C = 94$ K) of $CoCr_2O_4$ we observe a $\omega \sim 16$ cm^{-1} $\boldsymbol{q} = 0$ magnon having T_{1g}-symmetry, which has the transformation properties of an axial vector. The anomalously large Raman intensity of the T_{1g}-symmetry magnon is characteristic of materials with a large magneto-optical response and likely arises from large magnetic fluctuations that strongly modulate the dielectric response in $CoCr_2O_4$. The Raman susceptibility of the T_{1g}-symmetry magnon exhibits a strong magnetic-field dependence that is consistent with the magnetodielectric response observed in $CoCr_2O_4$, suggesting that magnetodielectric behavior in $CoCr_2O_4$ primarily arises from the field-dependent suppression of magnetic fluctuations that are strongly coupled to long-wavelength phonons. Increasing the magnetic anisotropy in $CoCr_2O_4$ with applied pressure decreases the magnetic-field dependence of the T_{1g}-symmetry magnon Raman susceptibility, suggesting that strain can be used to control the magnetodielectric response in $CoCr_2O_4$.

DOI: 10.1103/PhysRevB.95.174413

I. INTRODUCTION

Multiferroics—materials exhibiting a coexistence of both magnetic and ferroelectric orders [1,2]—have attracted substantial technological and scientific interest recently. The technological interest stems from the multifunctional properties exhibited by multiferroics, which make them potentially useful in device applications such as magnetoelectric memories and switches. Multiferroics are scientifically interesting, in part, because they exhibit a variety of microscopic mechanisms that can result in an interesting interplay between ferroelectric and magnetic orders [2]; among other consequences, this interplay can spawn interesting dynamical properties in multiferroic materials, including electromagnons, i.e., hybrid excitations involving a coupling between optical phonons and spin waves via the magnetoelectric interaction [3–14], and magnetodielectric effects [15–17].

Materials in which geometric frustration leads to noncollinear spin order and strong spin-lattice coupling are particularly rich material environments to find novel magnetoelectric behavior [1,18]. Transition-metal-oxide spinel materials (AB_2O_4), for example, exhibit both noncollinear spin orders and strong spin-lattice coupling that can lead to magnetoelectric coupling, because the presence of magnetic ions on the *B*-site pyrochlore lattice of the spinel structure often leads to strong geometric frustration and consequent noncollinear orders that can generate multiferroic phenomena [2]. Magnetoelectric effects are indeed realized in some ACr_2O_4 spinels (e.g., $A = Co^{2+}$ and Fe^{2+}), in which the competition among the various exchange interactions, $J_{A\text{-}A}$, $J_{A\text{-}Cr}$, and $J_{Cr\text{-}Cr}$, involving the A^{2+} ions and the Cr^{3+} $S = 3/2$ spins lead to complex magnetic orders [19,20]. $CoCr_2O_4$, in particular, exhibits a succession of magnetic orders, including ferrimagnetic order below $T_C = 94$ K, incommensurate conical spiral order below $T_S = 26$ K, and commensurate order below $T_L = 14$ K [21,22], as well as spin-driven multiferroic behavior and dielectric anomalies below T_S [23–25]. Yet, the nature and origin of magnetoelectric behavior in $CoCr_2O_4$ remains uncertain. Multiferroicity in $CoCr_2O_4$ has been associated with the spin-current mechanism [26] involving cycloidal spin order [23], in which the induced electric polarization is generated by the noncollinear spins [27] via the inverse Dzyaloshinskii-Moriya interaction, $\boldsymbol{P} \propto \boldsymbol{e}_{ij} \times (\boldsymbol{S}_i \times \boldsymbol{S}_j)$.

But evidence for multiferroicity [17,20], structural distortion [17], and magnetodielectric behavior [17] have also been reported above T_S in the ferrimagnetic state of $CoCr_2O_4$. Yang *et al.*, for example, have suggested that the observation of magnetodielectric behavior in $CoCr_2O_4$ well into the ferrimagnetic phase above T_S results from the presence of multiferroic domains that are reoriented in the presence of a magnetic field [17]. But magnetodielectric behavior in magnetic materials can also arise from magnetic fluctuations that induce shifts in optical phonon frequencies via strong spin-lattice coupling [16].

The focus of this study is on the origin of the magnetodielectric behavior in the ferrimagnetic phase above T_S in $CoCr_2O_4$. Unfortunately, a lack of microscopic information regarding

*asethi8@illinois.edu
†slcooper@illinois.edu

spin-lattice coupling has prevented a clear identification of the mechanism for magnetodielectric behavior in $CoCr_2O_4$. The intersublattice exchange magnon has been observed in $CoCr_2O_4$ using infrared and terahertz spectroscopies [28,29], and optical phonons in $CoCr_2O_4$ have been identified using Raman scattering [30–32] and optical absorption [28] measurements. However, these studies did not address the microscopic origin of the magnetodielectric behavior in the ferrimagnetic phase ($T < T_C$) of $CoCr_2O_4$. The application of pressure [33–35] would be a useful means of studying spin-lattice coupling and its role in magnetodielectric behavior in spinels such as $CoCr_2O_4$. Some *ab initio* calculations have been conducted that predict the effect of pressure on the magnetic exchange constants in $CoCr_2O_4$ [32]. However, the effects of pressure on the magnetodielectric behavior and spin-lattice coupling in $CoCr_2O_4$ have not yet been experimentally investigated.

In this paper, we present Raman scattering evidence for dielectric anomalies and magnetodielectric behavior driven by magnetic fluctuations and strong spin-phonon coupling in the ferrimagnetic phase of $CoCr_2O_4$. Raman scattering is a powerful tool for studying magnons [36,37], strong spin-lattice coupling [36,38], and electromagnons [39–42] in complex oxide materials. When used in conjunction with pressure and magnetic-field tuning, Raman scattering can provide pressure- and magnetic-field-dependent information about the energy and lifetime of phonons, magnons, and spin-phonon coupling effects. Most significantly, magnon Raman scattering intensities are associated with the modulation of the dielectric response by spin fluctuations [43–45], and consequently, magnetic-field-dependent studies of magnon Raman intensities provide a unique means of studying magnon contributions to the magnetodielectric response [43].

In this paper, we report an inelastic light (Raman) scattering study of magnon and phonon excitations in $CoCr_2O_4$ as simultaneous functions of temperature, pressure, and magnetic field. Below $T_C = 94$ K, we report the development in $CoCr_2O_4$ of a $\omega \sim 16$ cm^{-1} (2 meV) $\boldsymbol{q} = 0$ magnon excitation with T_{1g} symmetry. The anomalously large Raman scattering susceptibility associated with the T_{1g} symmetry magnon in $CoCr_2O_4$ is indicative of a large magneto-optical response arising from large magnetic fluctuations that couple strongly to the dielectric response. This result is consistent with the presence of dielectric anomalies associated with strong spin-phonon coupling in the ferrimagnetic phase of $CoCr_2O_4$. In support of this interpretation, we show that the Raman intensity of the T_{1g}-symmetry magnon in $CoCr_2O_4$ exhibits a strong suppression with increasing magnetic field, suggesting that the dramatic magnetodielectric behavior [17,46] observed in $CoCr_2O_4$ results from the magnetic-field-induced suppression of magnetic fluctuations that are strongly coupled to phonons [16]. Using applied pressure to increase the magnetic anisotropy in $CoCr_2O_4$ results in a decreased magnetic field dependence of the T_{1g}-symmetry magnon Raman intensity in $CoCr_2O_4$, suggesting that pressure or epitaxial strain can be used to control magnetodielectric behavior and the magneto-optical response in $CoCr_2O_4$ by suppressing magnetic fluctuations and the degree to which they modulate the dielectric response.

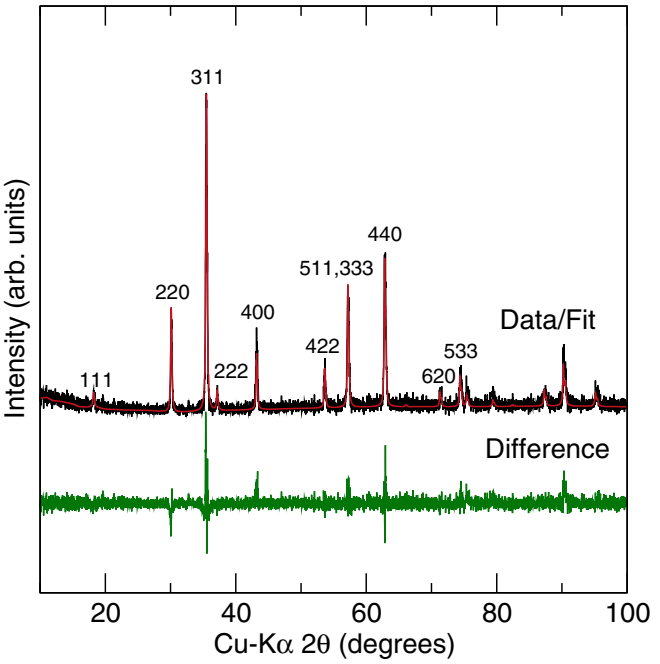

FIG. 1. X-ray diffraction pattern and Rietveld fit of $CoCr_2O_4$ at $T = 298$ K. The Miller indices for a cubic unit cell with cell parameter $a = 8.334(1)$ Å are also shown.

II. EXPERIMENTAL METHODS

A. Crystal growth and characterization

$CoCr_2O_4$ crystals were grown by chemical vapor transport (CVT) following a procedure described by Ohgushi *et al.* [47]. Polycrystalline powder samples of $CoCr_2O_4$ were first synthesized using cobalt nitrate hexahydrate (Strem Chemicals 99%) and chromium nitrate nonahydrate (Acros 99%). The nitrates were combined in stoichiometric amounts and dissolved in water. The solution was heated to 350 °C and stirred using a magnetic stir bar at 300 rpm until all of the liquid evaporated. The remaining powder was heated in an alumina crucible at 900 °C for 16 hours and then air quenched. Crystal samples of $CoCr_2O_4$ were grown by CVT using $CrCl_3$ as a transport agent. 2.0 g of polycrystalline samples and 0.04 g of $CrCl_3$ were sealed in an evacuated quartz ampoule, which was placed inside a three-zone furnace having 950°C at the center with a temperature gradient of 10 °C/cm for one month. Crystals with typical dimensions of $2 \times 2 \times 2$ mm^3 were obtained.

The $CoCr_2O_4$ crystals were characterised using x-ray diffraction and magnetization measurements. Crystals of $CoCr_2O_4$ were ground to a powder to obtain the x-ray diffraction pattern using a Siemens-Bruker D5000 diffractometer using Cu-Kα radiation shown in Fig. 1. Rietveld refinement of the $CoCr_2O_4$ cell to the XRD data was performed using XND Rietveld [48] and indicates a pure sample with $Fd\bar{3}m$ symmetry and a lattice constant of 8.334(1) Å, which agrees with the established structure [28]. The ⟨110⟩ reflections from a single crystal of $CoCr_2O_4$ were measured, and no evidence of twinning imperfections was found. The field-cooled dc magnetization data on the $CoCr_2O_4$ powder from which our crystal sample was obtained was collected using a Quantum Design MPMS-3 and is shown as a function of temperature

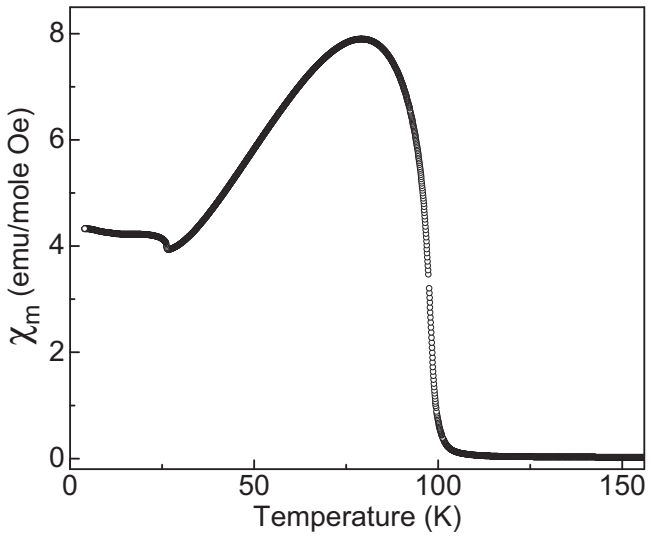

FIG. 2. Molar susceptibility of $CoCr_2O_4$ powder as a function of temperature measured in an applied field of 100 Oe.

in Fig. 2. Our results are similar to existing data [24]. In particular, the sudden increase in the molar susceptibility, χ_m, at $T = 94$ K marks the onset of ferrimagnetic ordering. The change in slope of the graph at $T = 26$ K and an additional small anomaly at $T = 14$ K correspond to the incommensurate and commensurate spiral ordering, respectively, in $CoCr_2O_4$.

B. Raman scattering measurements

Raman scattering measurements were performed using the 647.1 nm excitation line from a Kr^+ laser. The incident laser power was limited to 5–10 mW and was focused to a ~50-μm-diameter spot to minimize laser heating of the sample. Sample heating by the laser was estimated to be in the range of 5–7 K, and this estimated laser heating is included in the temperatures given in the results section. The scattered light from the samples was collected in a backscattering geometry, dispersed through a triple stage spectrometer, and then detected with a liquid-nitrogen-cooled CCD detector. The samples were inserted into a continuous He-flow cryostat, which was horizontally mounted in the open bore of a superconducting magnet [49]. This experimental arrangement allows Raman scattering measurements under the simultaneous conditions of low temperature (3–300 K), high magnetic field (0–9 T), and high pressures (0–100 kbar). To determine the symmetries of the measured Raman excitations in zero magnetic field, linearly polarized incident and scattered light were used for various crystallographic orientations of the sample. In the magnetic field measurements, circularly polarized light was used to avoid Faraday rotation of the light polarization.

Magnetic field measurements were performed in both Faraday ($\boldsymbol{k} \parallel \boldsymbol{M} \parallel \boldsymbol{H}$) and Voigt ($\boldsymbol{k} \perp \boldsymbol{M} \parallel \boldsymbol{H}$) geometries as illustrated in Fig. 3(d), where $\boldsymbol{k}$ is the wave vector of the incident light, $\boldsymbol{M} = \boldsymbol{M}_1 + \boldsymbol{M}_2$ is the total magnetization composed of the Co^{2+} and Cr^{3+} sublattice magnetizations, $\boldsymbol{M}_1$ and $\boldsymbol{M}_2$, respectively, $\boldsymbol{E}$ is the electric field polarization direction of the incident light, $\boldsymbol{H}$ is the applied magnetic field [49], and $\boldsymbol{L} = \boldsymbol{M}_1 - \boldsymbol{M}_2$ is the antiferromagnetic ordering

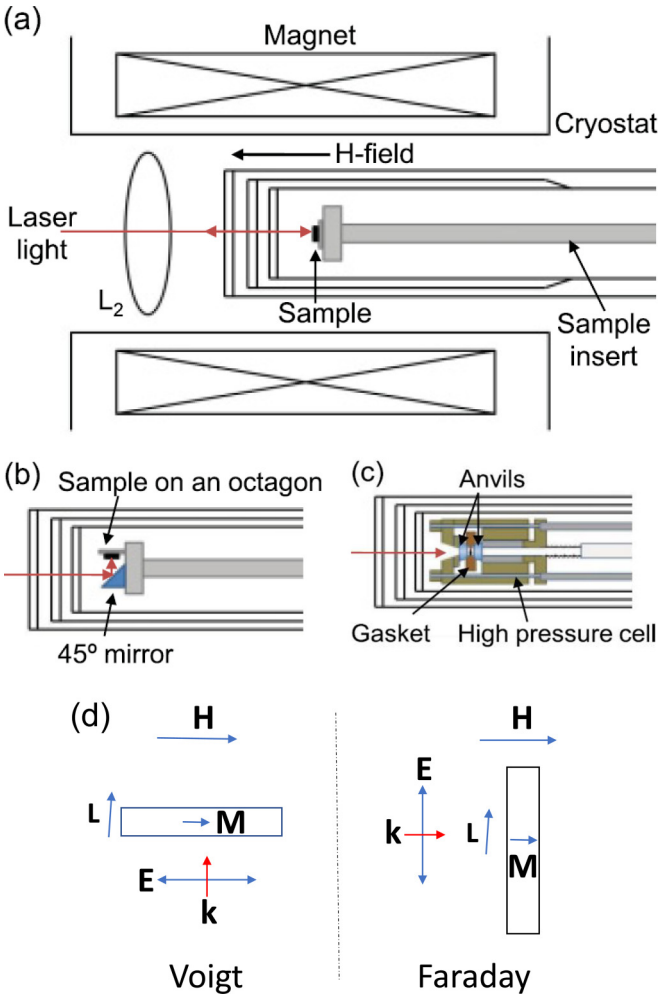

FIG. 3. Illustrations showing the experimental arrangements used for different high-magnetic-field and high temperature Raman scattering experiments at low temperatures in this study [49]. (a) Configuration for high-magnetic field measurements in the Faraday ($\boldsymbol{k} \parallel \boldsymbol{H}$) geometry, where $\boldsymbol{k}$ is the wave vector of the incident light and $\boldsymbol{H}$ is the applied magnetic field direction. (b) Configuration for high-magnetic-field measurements in the Voigt ($\boldsymbol{k} \perp \boldsymbol{H}$) geometry. (c) Configuration for high pressure measurements using a diamond anvil cell. (d) Schematic representation of the magnetization vectors and applied field in the Voigt (left) and Faraday (right) geometries.

vector. Because of the very small anisotropy field in $CoCr_2O_4$ ($H_A \leqslant 0.1$ T) [29], the net magnetization $\boldsymbol{M}$ was assumed to follow the applied field $\boldsymbol{H}$ in all experiments performed. To verify this, we confirmed that the field dependence of the Raman spectrum was independent of the crystallographic orientation of the applied field. The field measurements in the Faraday geometry were performed by mounting the sample at the end of the insert, as illustrated in Fig. 3(a), so that the wave vector of the incident light is parallel to the applied field. The Voigt geometry was achieved by mounting the sample on an octagon plate, which was mounted sideways on the sample rod, as illustrated in Fig. 3(b). The incident light was guided to the sample surface with a 45° mirror mounted on the sample rod. This sample mounting arrangement allows the magnetic field to be applied perpendicular to the wave vector of the incident light, $\boldsymbol{k} \perp \boldsymbol{M} \parallel \boldsymbol{H}$.

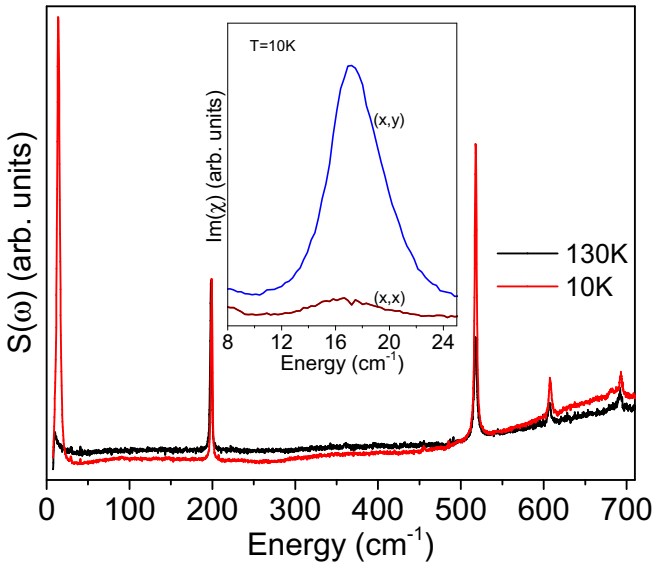

FIG. 4. Temperature dependence of the Raman scattering intensity, $S(\omega)$, for $CoCr_2O_4$ at $T = 10$ K and $T = 130$ K, showing the phonon modes above $\omega = 150\ \mathrm{cm}^{-1}$ and the T_{1g} symmetry magnon near $\omega = 16\ \mathrm{cm}^{-1}$ that evolves for $T < 90$ K. Inset shows the polarization dependence of the magnon in $CoCr_2O_4$; the presence of this mode only in the depolarized geometry for all crystallographic orientations is indicative of the T_{1g} symmetry, which transforms like an axial vector.

High pressure measurements were performed using a miniature cryogenic diamond anvil cell (MCDAC) to exert pressure on the sample via an argon liquid medium. The high-pressure cell was inserted into the cryostat as illustrated in Fig. 3(c), allowing the pressure to be changed *in situ* at low temperatures without any extra warming/cooling procedure. This arrangement allows simultaneous high-pressure and high-magnetic field measurements in the Faraday ($\boldsymbol{k} \parallel \boldsymbol{M} \parallel \boldsymbol{H}$) geometry, as illustrated in Fig. 3(c) [49]. The pressure was determined from the shift in the fluorescence line of a ruby chip loaded in the cell along with the sample piece.

The T_{1g}-symmetry magnon energy of $CoCr_2O_4$ varied slightly ($<1.5\ \mathrm{cm}^{-1}$) in some samples. Consequently, to avoid sample dependence effects, all field-dependent measurements in the Faraday geometry, as well as all the pressure-dependent measurements, were performed on the same sample with the laser focused to a specific spot on that sample. The temperature-dependent data in Fig. 4 and the Voigt-geometry field-dependent data plotted in Fig. 6(c) were measured on different samples. For the field measurements, it was found that the intensity of the $\omega = 199\ \mathrm{cm}^{-1}$ T_{2g} phonon was independent of field (see Sec. IV). Consequently, to account for small day-to-day variations in the experimental conditions, for field sweep measurements at a particular temperature and pressure, the field-dependent Raman spectra shown in the paper have been normalized to the Raman susceptibility of the $199\ \mathrm{cm}^{-1}$ T_{2g} phonon. Additionally, there were no significant systematic changes in the Raman susceptibility of the $199\ \mathrm{cm}^{-1}$ T_{2g} phonon in the pressure range 0–25 kbar, and consequently, to minimize the effects of day-to-day variations in the experimental conditions, the pressure-dependent Raman spectra shown at zero magnetic field were also normalized to the Raman susceptibility of the $199\ \mathrm{cm}^{-1}$ T_{2g} phonon (see Sec. V). The integrated Raman scattering intensities shown in this paper were determined by calculating the area (using Simpson's rule) under the Raman scattering susceptibility versus energy curves.

III. TEMPERATURE DEPENDENCE OF THE MAGNETIC EXCITATION AT $P = 0$ AND $B = 0$

A. Results

Figure 4 shows the $T = 10$ K and $T = 130$ K Raman spectra of $CoCr_2O_4$ in the energy range $0 < \omega < 700\ \mathrm{cm}^{-1}$ in a scattering geometry with circularly polarized incident light and unanalyzed scattered light. The $T = 10$ K spectrum exhibits the five Raman-active phonon modes expected and previously observed [30–32] for $CoCr_2O_4$, including phonon modes at $\omega = 199, 454, 518, 609$, and $692\ \mathrm{cm}^{-1}$ (at $T = 10$ K). In addition to the phonon modes, the $T = 10$ K spectrum in Fig. 4 has an additional mode that develops near $\omega \sim 16\ \mathrm{cm}^{-1}$ ($\sim$2 meV) below $T = 90$ K. The inset of Fig. 4 shows that the $\omega \sim 16\ \mathrm{cm}^{-1}$ mode intensity is present only in the "depolarized" scattering geometry, i.e., only when the incident and scattered light polarizations are perpendicular to one another, independent of the crystallographic orientation. This polarization dependence indicates that the $\omega \sim 16\ \mathrm{cm}^{-1}$ mode symmetry transforms like the fully antisymmetric representation, T_{1g}, which has the symmetry properties of an axial vector, characteristic of a magnetic excitation [50,51]. Consequently, we identify the $\omega \sim 16\ \mathrm{cm}^{-1}$ excitation as a $\boldsymbol{q} = 0$ T_{1g} symmetry magnon in $CoCr_2O_4$. This interpretation is supported by the temperature dependence of the $\omega \sim 16\ \mathrm{cm}^{-1}$ T_{1g}-symmetry mode Raman scattering susceptibility, Im $\chi(\omega)$ [see Fig. 5(a)], where $\mathrm{Im}\,\chi(\omega) = S(\boldsymbol{q} = 0, \omega)/[1 + n(\omega, T)]$, $S(\boldsymbol{q} = 0, \omega)$ is the measured Raman scattering response, and $n(\omega, T) = [e^{\hbar\omega/k_B T}) - 1]^{-1}$ is the Bose thermal factor.

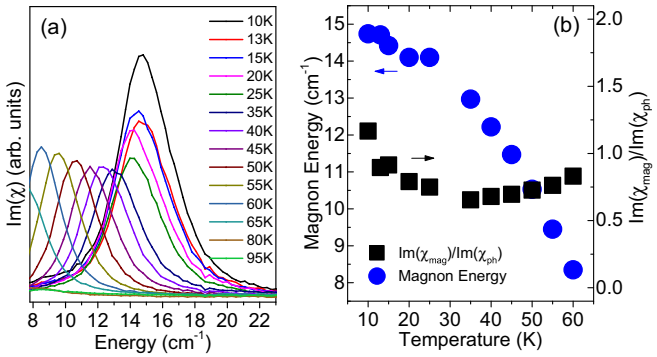

FIG. 5. (a) Raman scattering susceptibility, Im $\chi(\omega)$ (Im $\chi(\omega) = S(\boldsymbol{q} = 0, \omega)/[1 + n(\omega, T)]$, $S(\boldsymbol{q} = 0, \omega)$ is the measured Raman scattering response, and $n(\omega, T) = [e^{\hbar\omega/k_B T} - 1]^{-1}$ is the Bose thermal factor) of the T_{1g}-symmetry magnon of $CoCr_2O_4$ as a function of temperature. (b) Summary of the temperature dependence of the T_{1g} symmetry magnon energy (filled circles). Also shown in filled squares is a summary of the temperature dependence of the T_{1g} symmetry magnon Raman susceptibility amplitude normalized to the susceptibility amplitude of the $\omega = 199\ \mathrm{cm}^{-1}$ T_{2g} optical phonon, Im $\chi_{\mathrm{mag}}(\omega)$/Im $\chi_{ph}(\omega)$.

Figure 5(b) shows that the $\omega \sim 16\ \mathrm{cm}^{-1}$ T_{1g} symmetry mode energy (filled circles) decreases in energy ("softens") with increasing temperature toward T_C—consistent with the temperature dependence of the Co^{2+} sublattice magnetization [29]—indicative of a single-magnon excitation [50].

Notably, the $\omega \sim 16\ \mathrm{cm}^{-1}$ T_{1g} symmetry magnon we observe in $CoCr_2O_4$ has a similar energy and temperature dependence to that of the exchange magnon observed previously in terahertz [28] and infrared spectroscopy [29] measurements of $CoCr_2O_4$. In the collinear ferrimagnetic phase of $CoCr_2O_4$, the structure is presumed to be centrosymmetric, and thus infrared measurements should not be able to observe Raman-active modes and vice versa. Consequently, we believe that the T_{1g} magnon we observe in $CoCr_2O_4$ is unlikely to be the same mode observed in infrared and terahertz measurements, because a T_{1g} symmetry mode is not an infrared-active mode. Note in this regard that the spinel structure of $CoCr_2O_4$ is expected to exhibit six $q = 0$ magnon modes with five closely spaced optical branches [28,52–54]. Consequently, we are likely observing a different optical magnon that is close in energy to that observed in infrared measurements. An alternative possibility is that the appearance of the same magnon mode in both infrared and Raman measurements reflects a local breaking of symmetry into a noncentrosymmetric structure, even in the collinear ferrimagnetic phase. However, this alternative is unlikely, as we do not observe any additional (e.g., infrared-active) phonon modes that would indicate a locally noncentrosymmetric structure in the ferrimagnetic phase of $CoCr_2O_4$.

Importantly, the T_{1g} symmetry of the magnon we observe in $CoCr_2O_4$ is not predicted by the spin-wave calculation presented in Torgashev *et al.* [28] Our data suggests that the T_{1g} magnon mode in the ferrimagnetic phase is dominated by the precession of the Co^{2+} spins with negligible contributions from the Cr^{3+} sublattice, in agreement with previous findings [28,29]. This suggests that revised spin-wave calculations with weak coupling between the Co^{2+} and Cr^{3+} sublattices in the ferrimagnetic phase of $CoCr_2O_4$ are needed to account for our observation of a T_{1g} symmetry magnon in $CoCr_2O_4$.

B. Discussion and analysis

The finite $\boldsymbol{q} = 0$ energy of the $\omega \sim 16\ \mathrm{cm}^{-1}$ (2 meV) T_{1g} magnon in $CoCr_2O_4$ primarily reflects the finite exchange, H_E, and anisotropy, H_A, fields in $CoCr_2O_4$, according to $\omega = \gamma(2H_AH_E + {H_A}^2)^{1/2}$, where γ is the gyromagnetic ratio $g\mu_B/\hbar$ [51]. Figure 5 also shows that the $\omega \sim 16\ \mathrm{cm}^{-1}$ T_{1g} symmetry magnon in $CoCr_2O_4$ is apparent to temperatures as high as $T \sim 60$ K, indicating that the T_{1g} symmetry magnon in $CoCr_2O_4$ is dominated by the Co^{2+} sublattice spins, which order at a significantly higher temperature (94 K) than the Cr^{3+} sublattice (49 K) [29].

Importantly, the Raman susceptibility of the $\omega \sim 16\ \mathrm{cm}^{-1}$ T_{1g} symmetry magnon at $T = 10$ K (for $H = 0$ T and $P = 0$ kbar) (see Fig. 5) reflects the degree to which this magnon modulates the dielectric response, $\epsilon = 4\pi\chi_E$ (where χ_E is the electric susceptibility) [43,55]. Consequently, while Raman scattering from magnons is generally much weaker than Raman scattering from phonons [50], Figs. 4 and 5(b) show that Raman susceptibility of the T_{1g}-symmetry magnon is anomalously large, and in particular, is comparable to that of the $\omega = 199\ \mathrm{cm}^{-1}$ T_{2g} phonon in $CoCr_2O_4$.

The large Raman susceptibility of the T_{1g}-symmetry magnon in the ferrimagnetic phase is consistent with a large magneto-optical response in $CoCr_2O_4$ and is likely associated with strong magnetic fluctuations that modulate the dielectric response via strong spin-lattice coupling. Magnetic fluctuations are known to contribute to fluctuations in the dielectric response—and the associated magnon Raman intensity—in several ways [43–45]:

$$\delta\epsilon(\delta\boldsymbol{m},\delta\boldsymbol{l}) = i\ f\delta\boldsymbol{m} + g(\delta\boldsymbol{l})^2 + a(\delta\boldsymbol{m})^2, \qquad (1)$$

where $\delta\epsilon$ is the fluctuation of the dielectric response, $\delta\boldsymbol{m} = \boldsymbol{M} - \boldsymbol{M}_{\mathrm{st}}$ represents longitudinal fluctuations in the magnetization $\boldsymbol{M}$ from the static magnetization $\boldsymbol{M}_{\mathrm{st}}$, $\delta\boldsymbol{l} = \boldsymbol{L} - \boldsymbol{L}_{\mathrm{st}}$ represents fluctuations of the antiferromagnetic vector $\boldsymbol{L}$ from the static antiferromagnetic vector $\boldsymbol{L}_{\mathrm{st}}$, and a, f, and g are constants. The first term in Eq. (1) is associated with the linear magneto-optical Faraday effect, the second term is associated with linear magnetic birefringence, and the final term is an isotropic "exchange" mechanism for magnon scattering that is present in noncollinear antiferromagnets [43,56]. In noncollinear antiferromagnetic and ferrimagnetic materials with weak anisotropy and strong spin-phonon coupling—such as $CoCr_2O_4$—strong single-magnon scattering is expected to result from large fluctuations of both $\boldsymbol{M}$ and $\boldsymbol{L}$.

IV. MAGNETIC-FIELD DEPENDENCE OF THE T_{1g}-SYMMETRY MAGNON IN $CoCr_2O_4$

A. Results

As discussed above, the strong T_{1g}-symmetry magnon Raman intensity of $CoCr_2O_4$ reflects the strong modulation of the dielectric response by this magnon. Consequently, magnetic-field-dependent studies of the magnon Raman intensity offer a unique means of directly studying the magnon contribution to the magnetodielectric response in $CoCr_2O_4$. Figures 6(a) and 6(b) show the magnetic-field dependence of the Raman susceptibility for the T_{1g}-symmetry magnon of $CoCr_2O_4$ at $P = 0$ kbar and $T = 10$ K with an applied magnetic field in both the [Fig. 6(a)] Faraday ($\boldsymbol{k} \parallel \boldsymbol{M} \parallel \boldsymbol{H}$) and [Fig. 6(b)] Voigt ($\boldsymbol{k} \perp \boldsymbol{M} \parallel \boldsymbol{H}$) geometries. Figure 6(c) summarizes the field dependences of the T_{1g}-symmetry magnon energy at both $T = 10$ K and $T = 55$ K, showing that the T_{1g}-symmetry magnon energy exhibits a linear increase with increasing field. The shift in the T_{1g}-symmetry magnon energy with field, $d\omega/d\mathrm{H} \sim 1.1\ \mathrm{cm}^{-1}/\mathrm{T}$, corresponds to a dimensionless ratio $\hbar\omega/\mu_B H = 2.4$. This ratio is close to the $T = 4$ K value of $\hbar\omega/\mu_B H = 2.5$ measured for the exchange magnon in $CoCr_2O_4$ [29] and is consistent with the gyromagnetic ratio of 2.2 for Co^{2+} [28,57].

The main result of the magnetic field dependence of the modulation of dielectric response by spins is summarized in Fig. 6(d), which compares the field dependence of the integrated intensity of the T_{1g}-symmetry magnon normalized to the integrated intensity of the $\omega = 199\ \mathrm{cm}^{-1}$ T_{2g} phonon in both the (filled circle and square) Faraday ($\boldsymbol{k} \parallel \boldsymbol{M} \parallel \boldsymbol{H}$) and (filled triangle) Voigt ($\boldsymbol{k} \perp \boldsymbol{M} \parallel \boldsymbol{H}$) geometries. Figure 6(d) shows that there is a substantial decrease in the normalized

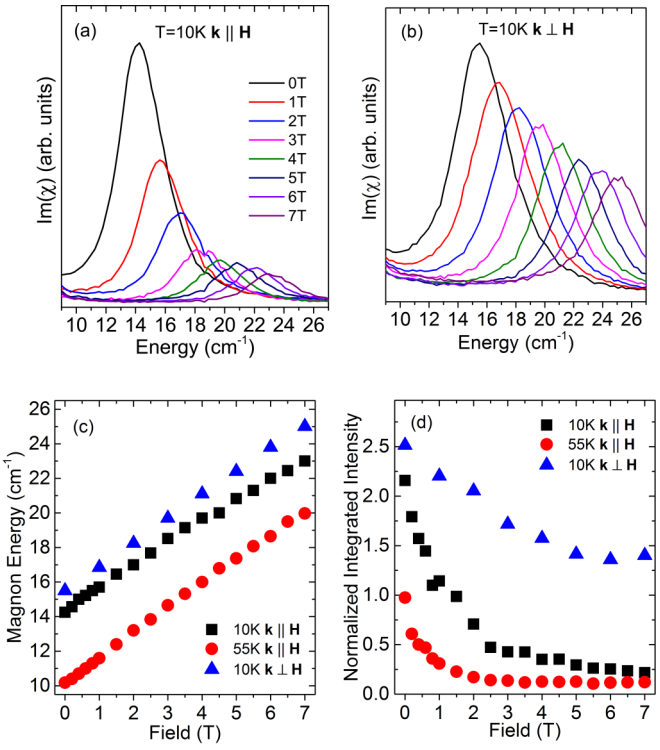

FIG. 6. Magnetic-field dependence of the Raman scattering susceptibility, Im $\chi(\omega)$, of the T_{1g}-symmetry magnon in $CoCr_2O_4$ at $T = 10$ K in the (a) Faraday geometry ($\boldsymbol{k} \parallel \boldsymbol{M} \parallel \boldsymbol{H}$) and the (b) Voigt geometry ($\boldsymbol{k} \perp \boldsymbol{M} \parallel \boldsymbol{H}$). (c) Summary of the field dependences of the T_{1g}-symmetry magnon energy of $CoCr_2O_4$ at (filled squares) $T = 10$ K and (filled circles) $T = 55$ K in the Faraday geometry and at (filled triangles) $T = 10$ K in the Voigt geometry. (d) Summary of the field dependences of the integrated intensity of the T_{1g}-symmetry magnon normalized to the integrated intensity of the $\omega = 199$ cm^{-1} T_{2g} phonon at (filled squares) $T = 10$ K and (filled circles) $T = 55$ K in the Faraday geometry and at (filled triangles) $T = 10$ K in the Voigt geometry.

integrated intensity of the T_{1g}-symmetry magnon of $CoCr_2O_4$ with increasing field in both the Faraday ($\boldsymbol{k} \parallel \boldsymbol{M} \parallel \boldsymbol{H}$) and Voigt ($\boldsymbol{k} \perp \boldsymbol{M} \parallel \boldsymbol{H}$) geometries at $T = 10$ K and $T = 55$ K. Figures 6(a) and 6(b) show that the linewidth broadening of the T_{1g} magnon peak with increasing magnetic field is not significant in $CoCr_2O_4$. Hence, the decrease in the integrated intensity of the magnon mode with increasing magnetic field indicates a field-dependent suppression of the magnon susceptibility. Note that the field-dependent decrease we observe in the T_{1g}-symmetry magnon Raman susceptibility—which is particularly dramatic in the Faraday geometry ($\boldsymbol{k} \parallel \boldsymbol{M} \parallel \boldsymbol{H}$)—cannot be attributed to field-dependent changes in polarization or crystallographic orientation: the T_{1g} symmetry of the magnon and the use of circularly polarized incident light in these experiments preclude the effect of any field induced rotations on the Raman intensity of the T_{1g} magnon.

B. Discussion and analysis

The large decrease in the $\omega \sim 16$ cm^{-1} T_{1g}-magnon Raman intensity with increasing field in the Faraday geometry ($\boldsymbol{k} \parallel \boldsymbol{M} \parallel \boldsymbol{H}$) of $CoCr_2O_4$ [see Fig. 6(c)] is quite different than the field-independent magnon Raman intensities observed in other spinel materials, such as Mn_3O_4 and MnV_2O_4 [36]. To understand the large T_{1g}-symmetry magnon Raman scattering intensity at $\boldsymbol{H} = 0$ and its decrease in a magnetic field, note that in the Faraday geometry [Fig. 3(d) (right))] the polarization of incident light couples primarily to dielectric fluctuations associated with the antiferromagnetic vector. The magnon Raman intensity in the Faraday geometry is therefore expected to be dominated by the linear magnetic birefringence contribution to dielectric fluctuations, $\delta\epsilon = g(\delta \boldsymbol{l})^2$ [see Eq. (1)] [43,45,56]. The size of antiferromagnetic vector fluctuations at $\boldsymbol{H} = 0$ is inversely related to the anisotropy field [43], H_A, which is very small in $CoCr_2O_4$ ($H_A \leqslant 0.1$ T) [29]. Consequently, the associated magnon Raman response is expected to be large in this scattering geometry. Further, the large field-dependent decrease in the T_{1g} magnon Raman intensity likely reflects a decrease in magnetic fluctuations—and a concomitant reduction in dielectric fluctuations [see Eq. (1)]—with applied magnetic field. A similar field-dependent decrease in the single-magnon inelastic light scattering response associated with fluctuations of the antiferromagnetic vector was also observed in the canted antiferromagnet EuTe [43].

Figure 6(b) shows that there is a similar, albeit less dramatic, field-dependent decrease in the T_{1g}-symmetry magnon Raman intensity measured in the Voigt ($\boldsymbol{k} \perp \boldsymbol{M} \parallel \boldsymbol{H}$) geometry. Figure 3(d) (left) shows that in this geometry, the incident polarization couples primarily to the longitudinal fluctuations in the magnetization $\delta \boldsymbol{m}$. This geometry is primarily sensitive to the Faraday ($\delta\epsilon = i\, f\, \delta \boldsymbol{m}$) contribution to dielectric fluctuations [see Eq. (1)] [43,45,56]. Altogether, the suppression of the T_{1g}-symmetry magnon Raman scattering intensities in both Faraday and Voigt geometries is consistent with a field-induced suppression of dielectric fluctuations associated with transverse and longitudinal magnetic fluctuations in $CoCr_2O_4$.

The field-dependent suppression of the T_{1g}-symmetry Raman intensity in $CoCr_2O_4$–which reflects a suppression of the magnetic fluctuations [see Eq. (1)]—points to a specific microscopic contribution to the magnetodielectric response observed in the ferrimagnetic phase of $CoCr_2O_4$. Lawes *et al.* have pointed out that the field-induced suppression of magnetic fluctuations can contribute to the magnetodielectric response of a material via the coupling of magnetic fluctuations to optical phonons [16]. This spin-phonon coupling contributes to the magnetodielectric response of a material through field-induced changes to the net magnetization [15–17,58]. Smolenskiĭ and Chupis [58] and others [15,17] have employed a simple phenomenological description for how the magnetization in a magnetodielectric material influences the material's dielectric response. In particular, these authors consider the free energy F in a magnetoelectric material with a coupling between the magnetization $\boldsymbol{M}$ and polarization $\boldsymbol{P}$ [15,17,58]:

$$F(M,P) = F_0 + aP^2 + bP^4 - PE + cM^2 + dM^4 - MH + eM^2P^2, \quad (2)$$

where F_0, a, b, c, d, and e are temperature-dependent constants, and M, P, E, and H are the magnitudes of the magnetization, polarization, applied electric field, and applied magnetic field, respectively. The resulting dielectric

response in a magnetodielectric material has been shown to depend inversely on the magnetization; consequently the dielectric response decreases with increasing magnetization [15,17,58]. This result is qualitatively consistent with our observation of the field-dependent suppression of the T_{1g} magnon Raman susceptibility in $CoCr_2O_4$, which indicates that the magnetic fluctuations that modulate the dielectric response are suppressed with an applied field.

Summarizing, the field-dependent decrease in the T_{1g}-symmetry Raman magnon intensity is likely related to the observed magnetodielectric response in $CoCr_2O_4$, as both reflect magnetic-field-induced changes to magnetic fluctuations that are strongly coupled to phonons [16] via the biquadratic contribution to the free energy, M^2P^2 [see Eq. (2)].

V. PRESSURE DEPENDENCE OF THE T_{1g}-SYMMETRY MAGNON IN $CoCr_2O_4$

A. Results

As discussed above, the strong T_{1g}-symmetry magnon Raman intensity of $CoCr_2O_4$ likely reflects strong magnetic fluctuations and the strong coupling of the spins to long-wavelength phonons. This strong T_{1g} magnon Raman response is also expected to be associated with significant linear Faraday and magnetic birefringence magneto-optical responses in $CoCr_2O_4$. Our results show that the application of a magnetic field suppresses magnetic fluctuations, contributing to the magnetodielectric response observed in $CoCr_2O_4$. An alternative approach to suppressing magnetic fluctuations and tuning spin-lattice coupling is to use applied pressure or strain to increase the crystalline anisotropy of $CoCr_2O_4$. To study the effects of pressure on the T_{1g}-symmetry magnon Raman intensity, pressure measurements at $\boldsymbol{H} = 0$ and magnetic-field-dependent measurements at various pressures of the T_{1g}-symmetry magnon in $CoCr_2O_4$ were performed.

Figure 7(a) shows the pressure dependence of the Raman susceptibility of the T_{1g} magnon in $CoCr_2O_4$ at $T = 10$ K and $\boldsymbol{H} = 0$ at various applied pressures, including $P =$ 0,4.5,15, and 21 kbar. Figure 7(b) summarizes the pressure dependence of the amplitude of the T_{1g}-symmetry magnon Raman susceptibility normalized to the amplitude of the $\omega = 199$ cm^{-1} T_{2g} phonon Raman susceptibility at $T = 10$ K and $\boldsymbol{H} = 0$ for different applied pressures, including $P =$ 0,4.5,15, and 21 kbar. We measured the pressure dependence of the T_{1g}-symmetry magnon energy on two different samples of $CoCr_2O_4$ at $H = 0$ and $T = 10$ K and our results are summarized in the inset of Fig. 7(b). Figures 7(c)–7(e) show the field dependence of the T_{1g}-symmetry magnon spectrum of $CoCr_2O_4$ in the Faraday ($\boldsymbol{k} \parallel \boldsymbol{M} \parallel \boldsymbol{H}$) geometry at $T = 10$ K for different applied pressures, including $P =$ 0,15, and 21 kbar.

Figure 8(a) shows the integrated intensity of the T_{1g}-symmetry magnon normalized to the integrated intensity of the $\omega = 199$ cm^{-1} T_{2g} phonon at $T = 10$ K for different applied pressures including $P = 0$,4.5,15, and 21 kbar. Figure 8(b) summarizes the field dependence of the T_{1g}-symmetry magnon energy at $T = 10$ K at various pressures specified in Fig. 8(a).

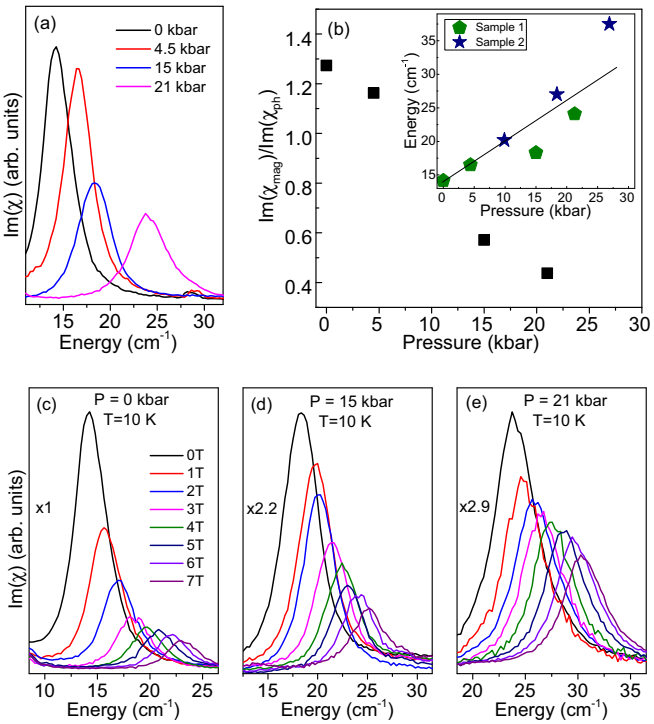

FIG. 7. (a) Pressure dependence of the T_{1g}-symmetry magnon Raman susceptibility of $CoCr_2O_4$ at $T = 10$ K and $\boldsymbol{H} = 0$ at various applied pressures, including $P = 0$,4.5,15, and 21 kbar. (b) Summary of the pressure dependence of the amplitude of the T_{1g}-symmetry magnon Raman susceptibility normalized to the amplitude of the $\omega = 199\,\text{cm}^{-1}$ T_{2g} phonon Raman susceptibility at $T = 10$ K and $\boldsymbol{H} = 0$ at various applied pressures, including $P = 0$,4.5,15, and 21 kbar. [(b) inset] Summary of the pressure dependence of the T_{1g}-symmetry magnon energy measured for two different samples of $CoCr_2O_4$ at $T = 10$ K and $\boldsymbol{H} = 0$. The two different samples of $CoCr_2O_4$, sample 1 and sample 2 are represented by filled pentagons and filled stars, respectively. (c)–(e) Field dependence in the Faraday ($\boldsymbol{k} \parallel \boldsymbol{M} \parallel \boldsymbol{H}$) geometry of the T_{1g}-symmetry magnon Raman susceptibility of $CoCr_2O_4$ at $T =$ 10 K and at various applied pressures, including (a) $P = 0$ kbar, (b) $P = 15$ kbar, and (c) $P = 21$ kbar.

B. Discussion and analysis

Figure 7(a) shows that the Raman susceptibility of the T_{1g} symmetry magnon in $CoCr_2O_4$ decreases with increasing pressure. In addition, Fig. 7(b) shows the systematic decrease in the T_{1g}-symmetry magnon Raman intensity relative to the T_{2g} phonon intensity at $H = 0$. This decrease can be attributed to a decrease in magnetic fluctuations and the degree to which these fluctuations modulate the dielectric response in $CoCr_2O_4$. Applied pressure is expected to increase both the anisotropy and exchange fields in $CoCr_2O_4$. While the available pressure-dependent data shown in the inset of Fig. 7(b) is sparse, the T_{1g}-symmetry magnon energy exhibits a roughly linear pressure dependence of $d\omega/dP \sim 0.6$ cm^{-1}/kbar over the range of pressures studied. This increase likely reflects a roughly linear increase in both the anisotropy and exchange fields, H_A and H_E, respectively, with increasing pressure, according to the relationship $\omega \propto (2H_AH_E)^{1/2}$. These results illustrate that increasing pressure suppresses the magnetic fluctuations

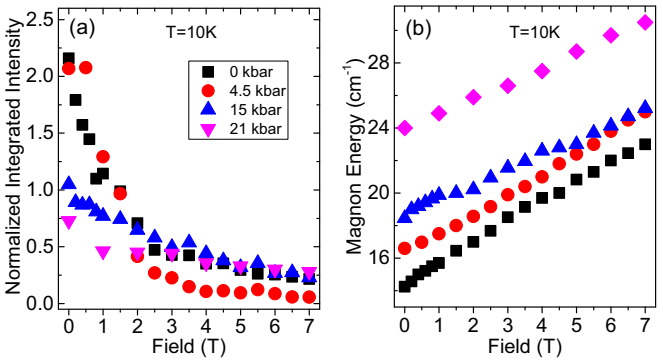

FIG. 8. (a) Summary of the field dependences of the integrated intensity of the T_{1g}-symmetry magnon normalized to the integrated intensity of the $\omega = 199$ cm^{-1} T_{2g} phonon at $T = 10$ K and various pressures, including (filled squares) $P = 0$ kbar, (filled circles) $P = 4.5$ kbar, (filled triangles) $P = 15$ kbar, and (filled diamonds) $P = 21$ kbar. (b) Summary of the field dependences in the Faraday ($\boldsymbol{k} \parallel \boldsymbol{M} \parallel \boldsymbol{H}$) geometry of the T_{1g}-symmetry magnon energy of $CoCr_2O_4$ at $T = 10$ K and at various pressures, including (filled squares) $P = 0$ kbar, (filled circles) $P = 4.5$ kbar, (filled triangles) $P = 15$ kbar, and (filled diamonds) $P = 21$ kbar.

and the magneto-optical response in $CoCr_2O_4$ by increasing the anisotropy field. Chen *et al.* have shown experimentally that with increasing pressure, the magnetization of $CoCr_2O_4$ increases [35]. This pressure dependence is consistent with the expectation that increasing crystalline anisotropy reduces the magnetic fluctuations and the associated dielectric fluctuations responsible for the T_{1g}-Raman magnon response [see Eq. (1)].

Figures 7 and 8 also show that increasing pressure reduces the strong suppression of the T_{1g}-symmetry magnon intensity with increasing magnetic field in the Faraday geometry ($\boldsymbol{k} \parallel \boldsymbol{M} \parallel \boldsymbol{H}$), indicating that the magnetodielectric response in the ferrimagnetic phase of $CoCr_2O_4$ should be suppressed with increasing pressure. Future magnetodielectric measurements in strained $CoCr_2O_4$ are needed to confirm this prediction. Additionally, the magnetic field dependence of the T_{1g}-magnon energy in $CoCr_2O_4$ at different fixed pressures summarized in Fig. 8(b) shows that the field-dependent slope associated with the T_{1g}-symmetry magnon frequency, $d\omega/dH$, is insensitive to applied pressure at least up to roughly 21 kbar, which is the highest pressure in our experiments, indicating that the gyromagnetic ratio associated with Co^{2+} is not strongly affected by these pressures in $CoCr_2O_4$. Altogether, our Raman scattering results show that, by tuning magnetic anisotropy and reducing magnetic fluctuations of the Co^{2+} spins, pressure and epitaxial strain can be used as effective tuning parameters for controlling the magnetodielectric response of $CoCr_2O_4$.

VI. SUMMARY AND CONCLUSIONS

In this paper, we showed that the $\boldsymbol{q} = 0$ T_{1g}-symmetry magnon in $CoCr_2O_4$ exhibits an anomalously large Raman scattering intensity, which reflects a large magneto-optical response that likely results from large magnetic fluctuations that couple strongly to the dielectric response. The strong suppression of the T_{1g}-symmetry magnon Raman intensity in an applied field is consistent with the magnetodielectric response observed in the ferrimagnetic phase of $CoCr_2O_4$ [17,46] and suggests that the strong magnetodielectric response is associated with the magnetic-field-induced suppression of magnetic fluctuations that are strongly coupled to phonons [16]. Using pressure to increase the magnetic anisotropy in $CoCr_2O_4$, we found that we can suppress the magnetic field dependence of the T_{1g}-symmetry magnon Raman intensity, demonstrating that pressure or epitaxial strain should be an effective means of controlling magnetodielectric behavior and the magneto-optical response in $CoCr_2O_4$. This Raman study also reveals conditions that are conducive for the substantial magneto-optical responses and magnetodielectric behaviors in materials, including the presence of strong spin-orbit coupling and weak magnetic anisotropy, both of which create favorable conditions for large magnetic fluctuations that strongly modulate the dielectric response.

ACKNOWLEDGMENTS

Research was supported by the National Science Foundation under Grant No. NSF DMR 1464090. R.D.M. and D.P.S. thank the Illinois Department of Materials Science and Engineering for support. X-ray diffraction and magnetic susceptibility measurements were performed in the Frederick Seitz Materials Research Laboratory.

[1] T. Kimura, T. Goto, H. Shintani, K. Ishizaka, T. Arima, and Y. Tokura, Nature (London) **426**, 55 (2003).
[2] S.-W. Cheong and M. Mostovoy, Nat. Mater. **6**, 13 (2007).
[3] V. G. Baryákhtar and I. E. Chupis, Sov. Phys. Solid State **11**, 2628 (1970).
[4] A. Pimenov, A. A. Mukhin, V. Y. Ivanov, V. D. Travkin, A. M. Balbashov, and A. Loidl, Nat. Phys. **2**, 97 (2006).
[5] N. Kida, Y. Ikebe, Y. Takahashi, J. P. He, Y. Kaneko, Y. Yamasaki, R. Shimano, T. Arima, N. Nagaosa, and Y. Tokura, Phys. Rev. B **78**, 104414 (2008).
[6] N. Kida, Y. Yamasaki, R. Shimano, T. hisa Arima, and Y. Tokura, J. Phys. Soc. Jpn. **77**, 123704 (2008).
[7] A. B. Sushkov, M. Mostovoy, R. V. Aguilar, S.-W. Cheong, and H. D. Drew, J. Phys.: Condens. Matter **20**, 434210 (2008).
[8] R. Valdés Aguilar, M. Mostovoy, A. B. Sushkov, C. L. Zhang, Y. J. Choi, S.-W. Cheong, and H. D. Drew, Phys. Rev. Lett. **102**, 047203 (2009).
[9] M. P. V. Stenberg and R. de Sousa, Phys. Rev. B **80**, 094419 (2009).
[10] M. Mochizuki, N. Furukawa, and N. Nagaosa, Phys. Rev. Lett. **104**, 177206 (2010).
[11] S. Tiwari and D. Sa, J. Phys.: Condens. Matter **22**, 225903 (2010).
[12] A. B. Harris, arXiv:1011.6672.

[13] S. P. P. Jones, S. M. Gaw, K. I. Doig, D. Prabhakaran, E. M. H. Wheeler, A. T. Boothroyd, and J. Lloyd-Hughes, Nat. Commun. **5**, 3787 (2014).

[14] K. Cao, F. Giustino, and P. G. Radaelli, Phys. Rev. Lett. **114**, 197201 (2015).

[15] T. Kimura, S. Kawamoto, I. Yamada, M. Azuma, M. Takano, and Y. Tokura, Phys. Rev. B **67**, 180401 (2003).

[16] G. Lawes, A. P. Ramirez, C. M. Varma, and M. A. Subramanian, Phys. Rev. Lett. **91**, 257208 (2003).

[17] S. Yang, H. X. Bao, D. Z. Xue, C. Zhou, J. H. Gao, Y. Wang, J. Q. Wang, X. P. Song, Z. B. Sun, X. B. Ren *et al.*, J. Phys. D **45**, 265001 (2012).

[18] T. Goto, T. Kimura, G. Lawes, A. P. Ramirez, and Y. Tokura, Phys. Rev. Lett. **92**, 257201 (2004).

[19] S. Bordács, D. Varjas, I. Kézsmárki, G. Mihály, L. Baldassarre, A. Abouelsayed, C. A. Kuntscher, K. Ohgushi, and Y. Tokura, Phys. Rev. Lett. **103**, 077205 (2009).

[20] K. Singh, A. Maignan, C. Simon, and C. Martin, Appl. Phys. Lett. **99**, 172903 (2011).

[21] K. Tomiyasu, J. Fukunaga, and H. Suzuki, Phys. Rev. B **70**, 214434 (2004).

[22] V. Tsurkan, S. Zherlitsyn, S. Yasin, V. Felea, Y. Skourski, J. Deisenhofer, H.-A. K. von Nidda, J. Wosnitza, and A. Loidl, Phys. Rev. Lett. **110**, 115502 (2013).

[23] Y. Yamasaki, S. Miyasaka, Y. Kaneko, J.-P. He, T. Arima, and Y. Tokura, Phys. Rev. Lett. **96**, 207204 (2006).

[24] G. Lawes, B. Melot, K. Page, C. Ederer, M. A. Hayward, T. Proffen, and R. Seshadri, Phys. Rev. B **74**, 024413 (2006).

[25] Y. J. Choi, J. Okamoto, D. J. Huang, K. S. Chao, H. J. Lin, C. T. Chen, M. van Veenendaal, T. A. Kaplan, and S.-W. Cheong, Phys. Rev. Lett. **102**, 067601 (2009).

[26] H. Katsura, N. Nagaosa, and A. V. Balatsky, Phys. Rev. Lett. **95**, 057205 (2005).

[27] M. Mostovoy, Phys. Rev. Lett. **96**, 067601 (2006).

[28] V. I. Torgashev, A. S. Prokhorov, G. A. Komandin, E. S. Zhukova, V. B. Anzin, V. M. Talanov, L. M. Rabkin, A. A. Bush, M. Dressel, and B. P. Gorshunov, Phys. Solid State **54**, 350 (2012).

[29] D. Kamenskyi, H. Engelkamp, T. Fischer, M. Uhlarz, J. Wosnitza, B. P. Gorshunov, G. A. Komandin, A. S. Prokhorov, M. Dressel, A. A. Bush *et al.*, Phys. Rev. B **87**, 134423 (2013).

[30] A. K. Kushwaha, Chin. J. Phys. **47**, 355 (2009).

[31] M. Ptak, M. Mączka, A. Pikul, P. Tomaszewski, and J. Hanuza, J. Solid State Chem. **212**, 218 (2014).

[32] I. Efthimiopoulos, Z. T. Y. Liu, S. V. Khare, P. Sarin, T. Lochbiler, V. Tsurkan, A. Loidl, D. Popov, and Y. Wang, Phys. Rev. B **92**, 064108 (2015).

[33] T. Kanomata, T. Tsuda, H. Yasui, and T. Kaneko, Phys. Lett. A **134**, 196 (1988).

[34] S. Tamura, Physica B: Condensed Matter **190**, 150 (1993).

[35] X. Chen, Z. Yang, Y. Xie, Z. Huang, L. Ling, S. Zhang, L. Pi, Y. Sun, and Y. Zhang, J. Appl. Phys. **113**, 17E129 (2013).

[36] S. L. Gleason, T. Byrum, Y. Gim, A. Thaler, P. Abbamonte, G. J. MacDougall, L. W. Martin, H. D. Zhou, and S. L. Cooper, Phys. Rev. B **89**, 134402 (2014).

[37] Y. Gim, A. Sethi, Q. Zhao, J. F. Mitchell, G. Cao, and S. L. Cooper, Phys. Rev. B **93**, 024405 (2016).

[38] T. Byrum, S. L. Gleason, A. Thaler, G. J. MacDougall, and S. L. Cooper, Phys. Rev. B **93**, 184418 (2016).

[39] M. Cazayous, Y. Gallais, A. Sacuto, R. de Sousa, D. Lebeugle, and D. Colson, Phys. Rev. Lett. **101**, 037601 (2008).

[40] M. K. Singh, R. S. Katiyar, and J. F. Scott, J. Phys.: Condens. Matter **20**, 252203 (2008).

[41] P. Rovillain, M. Cazayous, Y. Gallais, A. Sacuto, M.-A. Measson, and H. Sakata, Phys. Rev. B **81**, 054428 (2010).

[42] P. Rovillain, M. Cazayous, Y. Gallais, M.-A. Measson, A. Sacuto, H. Sakata, and M. Mochizuki, Phys. Rev. Lett. **107**, 027202 (2011).

[43] S. O. Demokritov, N. M. Kreines, and V. I. Kudinov, Sov. Phys. JETP **65**, 389 (1987).

[44] V. G. Baryakhtar, Y. G. Pashkevich, and V. L. Sobolev, Sov. Phys. JETP **58**, 945 (1983).

[45] A. S. Borovik-Romanov and N. M. Kreines, in *Spin Waves and Magnetic Excitations* (North-Holland, Amsterdam, 1988), Chap. 2.

[46] N. Mufti, A. A. Nugroho, G. R. Blake, and T. T. M. Palstra, J. Phys.: Condens. Matter **22**, 075902 (2010).

[47] K. Ohgushi, Y. Okimoto, T. Ogasawara, S. Miyasaka, and Y. Tokura, J. Phys. Soc. Jpn. **77**, 034713 (2008).

[48] J. Bérar and G. Baldinozzi, IUCr-CPD Newsletter **20**, 3 (1998).

[49] M. Kim, X. M. Chen, X. Wang, C. S. Nelson, R. Budakian, P. Abbamonte, and S. L. Cooper, Phys. Rev. B **84**, 174424 (2011).

[50] M. G. Cottam and D. J. Lockwood, *Light Scattering in Magnetic Solids* (Wiley-Interscience, New York, 1986).

[51] A. K. Ramdas and S. Rodriguez, Top. Appl. Phys. **68**, 137 (1991).

[52] J. Kaplan and C. Kittel, J. Chem. Phys. **21**, 760 (1953).

[53] W. F. Brinkman and R. J. Elliott, Proc. R. Soc. London A **294**, 343 (1966).

[54] V. Sahni and G. Venkataraman, Adv. Phys. **23**, 547 (1974).

[55] A. Kumar, J. F. Scott, and R. S. Katiyar, Appl. Phys. Lett. **99**, 062504 (2011).

[56] I. Vitebskii, A. Yeremenko, Y. Pashkevich, V. Sobolev, and S. Fedorov, Physica C: Superconductivity **178**, 189 (1991).

[57] S. A. Altshuler and B. M. Kozyrev, *Electron Paramagnetic Resonance in Compounds of Transition Elements* (Wiley, New York, 1974).

[58] G. A. Smolenskiĭ and I. E. Chupis, Sov. Phys. Usp. **25**, 475 (1982).